A&A manuscript no.
(will be inserted by hand later)

Your thesaurus codes are:
02(02.13.1; 02.09.1; 11.13.2; 11.19.2; 11.09.4; 09.11.1)

ASTRONOMY
AND
ASTROPHYSICS
22.2.2011

The galactic dynamo effect due to Parker-shearing instability of magnetic flux tubes

II. Numerical simulations and the nonlinear evolution.

M. Hanasz

Centre for Astronomy, Nicolaus Copernicus University, PL-87-148 Piwnice/Torun, Poland, (*mhanasz@astri.uni.torun.pl*)

Received November 26, 1996/ accepted May 29, 1997

Abstract. In this paper we continue investigations of the Parker-shearing instability performing numerical simulations of the magnetic flux tube dynamics in the thin flux-tube approximation. We show that evolution of flux tubes resulting from numerical simulations is very similar to that of linear solutions if the vertical displacements are smaller than the vertical scale height H of the galactic disc. If the vertical displacements are comparable to H, the vertical growth of perturbations is faster in the nonlinear range than in the linear one and we observe a rapid inflation of the flux tube at its top, which leads to a singularity in numerical simulations, if only the cosmic rays are taken into account. Then we perform simulations for the case of nonuniform external medium, which show that the dominating wavelength of the Parker instability is the same as the wavelength of modulations of external medium. As a consequence of this fact, in the case of dominating cosmic ray pressure, the dynamo α effect related to these short wavelength modulations is much more efficient than that related to the linearly most unstable long wavelengths modes of the Parker instability. Under the influence of differential forces resulting from differential rotation and the density waves, the α-effect is essentially magnified in the spiral arms and diminished in the interarm regions, what confirms our previous results obtained in the linear approximation.

Key words: Magnetic fields – Instabilities – Galaxies: magnetic fields – spiral – ISM: kinematics and dynamics of

1. Introduction

In the preceding paper (Hanasz and Lesch 1997, hereafter Paper I) we investigated the idea that the galactic dynamo action is driven by the Parker-shearing instability (Parker 1992, Hanasz & Lesch 1993, hereafter HL'93). We use the terms "Parker instability" or "Parker-shearing instability" depending on the context (i.e. on the current relevance of the rotational shearing effects). We presented the theory of slender magnetic flux tubes, analogous to that proposed by Spruit (1981), Spruit & Van Ballegooijen (1982) and Moreno-Insertis (1986), adopted to the case of galactic magnetic flux tubes. Then, performing the linear stability analysis we calculated the dynamo coefficients resulting from the Parker-shearing instability of magnetic flux tubes in the thin flux tube approximation. The calculations allowed us to derive a series of results which made conspicuous the power of the Parker-shearing instability as the mechanism generating the dynamo action (see Sect. 4. of Paper I).

It is obvious, however, that the linear approximation does not allow to inquire those aspect of the problem which are related to the evolution of perturbations for large amplitudes compared to the vertical scale height H. The problem results from the fact that the perturbations grow exponentially in the linear approximation and after a finite time period some physical quantities reach unphysical values. Since the possibilities of the extension of the work in the frame of analytical methods are rather limited, we decided to continue our studies by means of numerical simulations. We are going to present numerical solutions of the set of nonlinear equations describing the dynamics of flux tubes derived in Sect. 2 of Paper I together with the related dynamo transport coefficients. The solutions will allow us to verify the results of Paper I in the nonlinear regime and make a point to an old question about the final state of the Parker instability in galactic discs.

The problem of the final state of the Parker instability with and without cosmic rays has been discussed intensively in the past. Parker (1968, 1969) argues that cosmic rays leave the Galaxy by rapidly inflating bubbles on the magnetic field lines. This picture has been denied by

Send offprint requests to: M. Hanasz

Mouschovias (1974, 1975) who has shown that: 1) without cosmic rays the Parker instability attains final, curved equilibrium states and 2) the final equilibria are attained also in the presence of cosmic rays if only the number of cosmic ray particles within a particular flux tube is conserved during the flux tube motion. In this model the cosmic ray pressure is uniform along the magnetic field line and varies with the volume of the flux tube. These 2-dimensional solutions of Mouschovias have been tested with respect to instability against the perturbations in the 3-rd (radial) dimension by Asseo et al. (1978, 1980), Lechieze-Rey et al. (1980) and appeared to be unstable even without cosmic rays.

Some approaches to the Parker instability treated the cosmic ray gas as a relativistic gas, whose particles propagate with infinite speed along the magnetic field lines (see the discussion by Shu (1974) on this topic and references therein). It appears however, that the cosmic ray gas streaming along the magnetic field lines induces Alfven waves which exert a friction and slow the effective transport of cosmic rays down to the Alfven speed. Parker (1992) discusses his concept of inflating magnetic lobes, assuming explicitly that the inflation rate is limited by the Alfvenic streaming spend of the cosmic ray gas.

The assumption of Mouschovias on the conservation of the number of cosmic ray particles within the flux tube cannot be retained because of the high production rate of cosmic rays due to the supernova explosions. There are at least two observational facts which strongly support the Parkers point of view. 1) The measured cosmic ray lifetime 10^7 yr in galactic discs implies that the cosmic rays should disconnect from the disc together with the trapping magnetic field. The characteristic time scale of Parker instability $\sim 10^7$ yr is consistent with this point of view. 2) In some edge-on galaxies a vertical magnetic field is observed in radio continuum (Hummel et al. 1991; Golla and Hummel 1994) extending in galactic halos. One should mention that the Parker instability is invoked to explain the formation of vertical magnetic fields in the galactic halo, among the other models like galactic fountains (Kahn and Brett, 1993) and galactic winds (Spencer and Cram, 1992). We are going to point out however, that the Parker instability with the contribution of cosmic rays can serve as a fully sufficient explanation.

In HL'93 and Paper I we assumed that flux tubes are anchored at heavy molecular clouds. We have proposed that the typical intercloud distance determines the characteristic wavelength of the Parker instability. From Fig.5 of Paper I it follows that the range of unstable wavelengths depends on the magnetic pressure (via α). In the limit of weak magnetic field (e.g. $\alpha = 0.001$) the marginal stability point is far below the wavelength 100 pc, then the typical distance between clouds (~ 100 pc) corresponds to an unstable wavelength. Analogously, we can expect that even with the present magnetic field strength an instantaneous and local growth of the cosmic ray pressure due to supernova explosions can help to overcome the magnetic field tension and shift the marginal stability point below given intercloud distance. In such a case the dominating wavelength of Parker instability can be much smaller than the frequently invoked value of a few vertical scaleheights.

In the present section we generalize the physical setup and introduce a physically new effect - the propagation of flux tubes in an external medium which is nonuniform. The nonuniformities of the external medium are assumed to be spatially periodic and oscillating in time. It is our aim to check what is the evolution of a single flux tube in the nonuniform environment. The local and temporal external gas condensations are intended to imitate the clouds in the ambient medium. We assume that such clouds appear and disappear along the length of the flux tube modifying the external density only, but have not a dynamical influence on the flux tube. This seems to be quite difficult at present to treat consistently the flux tube – cloud, or flux tube – flux tube collisions. Such a local and temporal external density modulations influence the flux tube internal mass distribution via the magneto-hydrostatic balance condition (Eqn. (30) of Paper I). Variations of the external density distribution force a continuous mass redistribution inside the tube triggering the possible instabilities all over the flux tube lifetime, not only at the initial moment. In this respect our model seems to be more similar to of realistic interstellar medium than to the highly idealized uniform case. We are going to show that even a small amplitude external density modulations determine the characteristic wavelengths of the Parker modes. This in turn essentially influence the magnitude of the α-effect.

The effects of the galactic dynamics on the Parker instability has been discussed in Paper I in the linear approximation. The differential forces due to the axisymmetric differential rotation and the density waves influence essentially the dynamics of flux tubes as well as the dynamo transport coefficients. We found in Paper I that due to the presence of the radial differential force the curves of growth rate split into two separate parts at the wavenumber k_{crit} which is determined by the balance of the differential force, Coriolis force and the radial component of magnetic tension. In the range $k_{crit} < k < k_{marg}$ (the Parker range), where k_{marg} is the ordinary marginal stability point, the linear solutions are stationary growing, as in the case without shear and the α-effect is essentially magnified. In the range $0 < k < k_{crit}$ (the shearing range) the linear solutions behave like propagating waves and the α-effect is essentially diminished. We pointed out that the density waves can modify the differential force periodically with a relatively large amplitude, so that a perturbation with a given wavenumber placed in vicinity of k_{crit} can move from the Parker to shearing range and vice versa depending on the phase of the density wave. Since the Parker range corresponds to the spiral arms and the shearing range to the interarm regions we showed that the α-effect can switch on in arms and -off in the interarm

regions. We predict that the regular component should be stronger in the interarm regions than in the arms due to the simultaneous action of strong shear and the magnetic reconnection. These properties are very consistent with the observed arms of the uniform magnetic field in NGC 6946 (Beck and Hoernes 1996) placed in between the optical arms. We are going to verify the above results in the nonlinear range by means of the nonlinear numerical simulations.

The plan of this paper is as follows: In Section 2. we present the applied numerical method, Section 3 is devoted to the comparison of the numerical solutions with linear analytical solutions of Paper I. In Section 4 we analyze the final states of the Parker instability. In Section 5 we calculate the temporal evolution of the dynamo coefficients. In Section 6 the physical conditions are generalized by introducing modulations in the density of external medium, in which the flux tube propagate. In Section 7 we examine the influence of the effects of differential forces in the nonlinear regime on the flux tube evolution and the dynamo action. Conclusions and possible relations of our theoretical results to the observational results are contained in Section 8.

2. The method

In Paper I we have derived the system of MHD equations governing evolution of a slender magnetic flux tube in the thin flux tube approximation. Geometry of the thin flux tube and the equations of motion have been described in the Section 2. of Paper I. The system of partial differential equations describing evolution of the flux tube is given by equations (35), (36), (37) of Paper I for 9 unknown functions of time and position along the flux tube, together with the condition of magnetohydrostatic equilibrium of the flux tube with its surrounding (34). The unknown functions are: the Lagrangian coordinates of an element of the flux tube x, y, z, the components of the tangent vector L_x, L_y, L_z and the components of velocity v_x, v_y and v_z. We shall not rewrite these equations here for brevity. Since we are going to solve the system of partial differential equations by means of 1D numerical simulations we shall concentrate only on aspects related directly to this method.

We shall use the numerical algorithm PDECOL taken from the NETLIB library (algorithm 540R, Madsen & Sincovec 1992). The package PDECOL is based on the method of lines and uses a finite element collocation procedure (with piecewise polynomials as the trial space) for the discretization of the spatial variable x. The collocation procedure reduces the partial differential equation system to a semi-discrete system which then depends only on the time variable t. The time integration is then accomplished by use of standard techniques. The package solves the general system of nonlinear partial differential equations of at most second order of the form

$$\frac{\partial U}{\partial t} = F\left(t, x, U, \frac{\partial U}{\partial x}, \frac{\partial^2 U}{\partial x^2}\right) \tag{1}$$

with given boundary conditions and an initial condition. In our approach we shall apply the periodic boundary conditions and the initial conditions of two types. The first type will be given by an eigenmode resulting from the linear stability analysis. Such an initial state will allow to compare the linear analytical and the nonlinear numerical solutions. Results obtained with this initial state will serve for tests of the numerical algorithm. As the second type of the initial state we shall use a random superposition of periodic perturbations of the initial velocity and the vanishing initial displacements. Initial states of this type will allow for studies of the flux tube dynamics in conditions which more realistically resemble the nonuniform interstellar medium.

3. The comparison of analytical and numerical solutions

With the aim to test the correctness of the numerical solutions we shall compare them with the analytical linear solutions of the Paper I. First, we shall apply the initial state of a small amplitude, which is given by the linear solution with a wavenumber k and an amplitude Z_{init}. Then we shall observe the temporal evolution of the numerical and analytical solutions which both start from the same initial state. We expect that before the nonlinear effects become important, these two solutions should evolve accordingly. We are going to compare the linear and the nonlinear amplitudes of displacements of the flux tube gas in the three spatial directions at a given moment t_0. The linear solution will be represented by $X_l = |X_1|\exp(\omega_i t_0)$, $Y_l = |Y_1|\exp(\omega_i t_0)$ and $Z_l = |Z_1|\exp(\omega_i t_0)$. The numerical nonlinear solution will be represented by the appropriate quantities $X_n = \max|\Delta X(s,t_0)|$, $Y_n = \max|\Delta Y(s,t_0)|$ and $Z_n = \max|\Delta Z(s,t_0)|$, where $\Delta X(s,t_0)$, $\Delta Y(s,t_0)$ and $\Delta Z(s,t_0)$ are the Lagrangian displacements of an element of the flux tube with respect to its equilibrium position at the time t_0. The maxima are taken over a full range of variability of the length parameter s. An exemplary result obtained with the angular velocity typical for our Galaxy $\Omega = \Omega_G$, the Oort constant $A = 0$, the ratios of cosmic ray and magnetic pressures to the gas pressure $\alpha = \beta = 1$, the aerodynamic drag coefficient $C_D = 0$ and the wavelengths of the perturbation $H = 1330$ pc (representing the most unstable mode) is shown in Fig. 1. Throughout the paper the initial height of the azimuthal flux tube is $Z_0 = 100$ pc, which is comparable to a half of the typical vertical scaleheight ($H \sim 200$ pc). The other parameters, which are not mentioned explicitly are the same as those assumed in Paper I for our Galaxy.

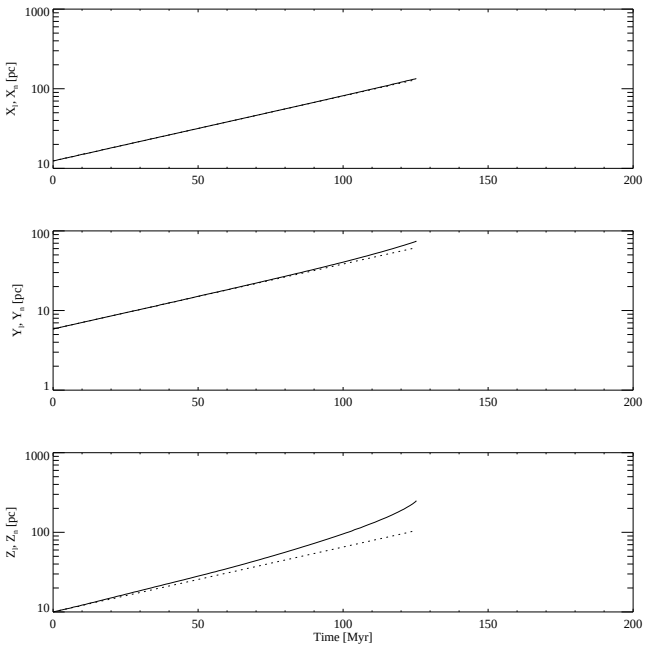

Fig. 1. The comparison of the nonlinear numerical solution (full line) to the linear analytical solution (dotted line). The amplitudes of displacements in three directions vs. time are plotted. The basic parameters are: $\Omega = \Omega_G$, $A = 0$, $\alpha = \beta = 1$, $\lambda = 1330$ pc and $C_D = 0$

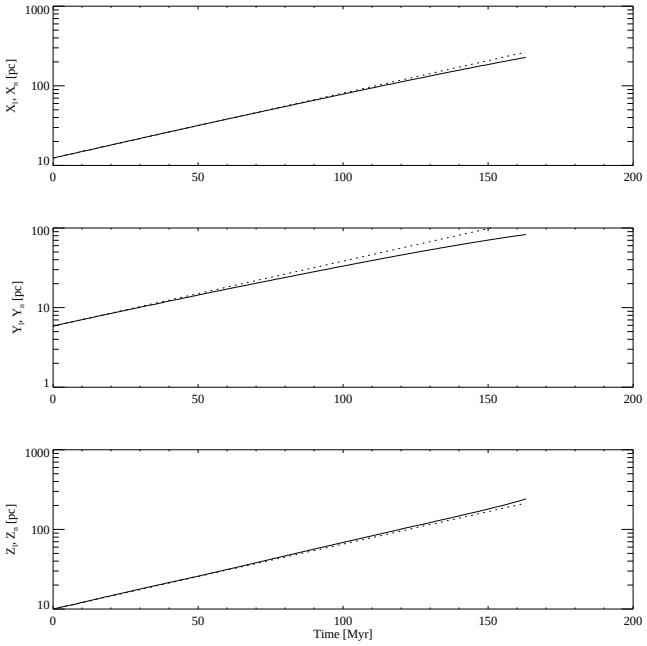

Fig. 2. The comparison of the nonlinear numerical solution (full line) to the linear analytical solution (dotted line). The amplitudes of displacements in three dimensions vs. time are plotted. Parameters like in Fig. 1 but $C_D = 1$ and $r = 10$ pc.

We note that the solutions are in a very good agreement especially concerning the coordinates x and y. However, a small discrepancy in the vertical direction is remarkable. The reason for this discrepancy is in the linear approximation of expression for the magnetic tension. Since in the linear approximation the curvature vector $\boldsymbol{K}$ has only the linear component, then the coefficient $B^2/4\pi\rho_i$ contributes only in the zeroth order. This means that we take in linear approximation B_0^2 instead of B^2, which is overestimated at the upward displaced parts of the flux tube, inflated due to the cosmic rays. Then the vertical component of the magnetic tension is diminished in the nonlinear regime with respect to the linear approximation. A similar argumentation applies also to the buoyancy term. This term is underestimated in the linear approximation. This explains why the top of the flux tube rises faster in numerical simulations than in the linear approximation. Thus, we can say that the numerical and analytical linear solutions are mutually consistent for relatively small vertical amplitudes $Z < H$. This allows us to expect that the basic conclusions of Paper I, essential for the dynamo theory remain invariable in the nonlinear regime for $Z < H$. We shall demonstrate in the next sections of this paper that this expectation is correct. Moreover, we shall be able to take into account some effects, which have not been tractable within the frame of the linear approximation.

As an example we shall examine the effect of aerodynamic drag force. HL'93 proposed that the aerodynamic drag force plays an important role for the dynamo transport coefficients, especially for the turbulent diffusivity. It was argued in that paper that the aerodynamic drag force slows down the vertical motions of fluxtubes and thereby diminishes the vertical diffusion of magnetic field. The discussion of the effect of the drag force has been omitted in Paper I since we focused our attention on the linear approximation and the resulting properties. Solving the flux tube equations by means of the nonlinear numerical simulations we are able to take the drag force into account. A corresponding solution with the parameter set as in Fig. 1 but with the aerodynamic drag force determined by the aerodynamic drag coefficient $C_D = 1$ and the flux tube radius $r = 10$ pc, is presented in Fig. 2.

It is apparent in Fig. 2 that with the given values of parameters, the aerodynamic drag force influences motion of the flux tube only moderately. One should be aware however that the assumed values of the drag coefficient and the flux tube radius are essentially model dependent. Moreover, the assumed physics underlying the aerodynamic drag effect may appear to be too simple for the case of galactic flux tubes. Nevertheless, one can notice that according to our expectations the drag force slows down the components of velocity perpendicular to the flux tube axis retaining the longitudinal velocity almost unchanged.

4. The final state of Parker instability

In this section we shall continue to examine the nonlinear evolution of modes, which are introduced to the numerical experiment as the linear initial states, as it was described in the previous section. The first point, which deserves a special attention, is related to the final states of our simulations. We note that the simulations brake down in a certain moment T_{end}. Moreover, we are not able to extend the simulations past T_{end} by making the grid resolution more tiny. Typically we divide the spatial domain – the full period of the perturbation into 200 grid cells. Even the division of the spatial domain into 5000 cells does not allow to extend simulations past T_{end}. The more frequent sampling of the numerical solutions allows to approach T_{end} closer and closer. In the following Figs. 3. and 4. we illustrate what happens. We plot all the most relevant physical variables: 3 components of the Lagrangian displacement of the flux tube, together with the 3 components of velocity and acceleration, the internal density ρ_i, the external density ρ_e, the strength of magnetic field B inside the tube, the mass per unit length ξ, the flux tube radius r and the ratio of the total speed to the Alfven speed $|v|/v_A$ as a function of position along the tube s. Fig. 3. and Fig. 4. show these quantities at $T = 125.0$ Myr and $T = 125.2$ Myr, respectively ($T_{end} < 125.3$ Myr).

We can easily notice that the internal density ρ_i approaches 0 at the top of flux tube at the moment directly preceding T_{end}, while the external density still remains nonvanishing. The vertical acceleration due to the buoyancy force starts to grow without limit within a limited time period. The appropriate panels of Figs. 3 and 4. apparently show this effect. All the other quantities behave regularly up to the moment T_{end}. It is worthwhile however, to have a look at the other panels too.

First of all, we notice that the topmost part of the tube starts to inflate (the flux tube radius r grows) at the time preceding T_{end}. We shall argue that the reason for this inflation is the cosmic ray pressure. We have assumed: 1) that the cosmic ray pressure is constant along the magnetic field lines and 2) that it is fixed at z_0 (as if the flux tube were connected to an infinite reservoir of cosmic rays at z_0). The gas density and pressure of the unperturbed disc decay exponentially with the increasing height z, thus at a certain height z_1 the total (gas + magnetic + cosmic ray) pressure equals to the cosmic ray pressure at the initial flux tube height z_0. The cosmic ray pressure inside the flux tube element displaced from z_0 to z_1 is the same as the one at z_0. Then, this is not possible to balance the internal cosmic ray pressure if the flux tube element is displaced further above z_1, where the surrounding total pressure is smaller than the cosmic ray pressure alone inside the raised element of the flux tube. This pressure imbalance has to result in a rapid inflation of the rising flux tube at its top. The inflation together with the outflow of the thermal gas from the top cause that the internal

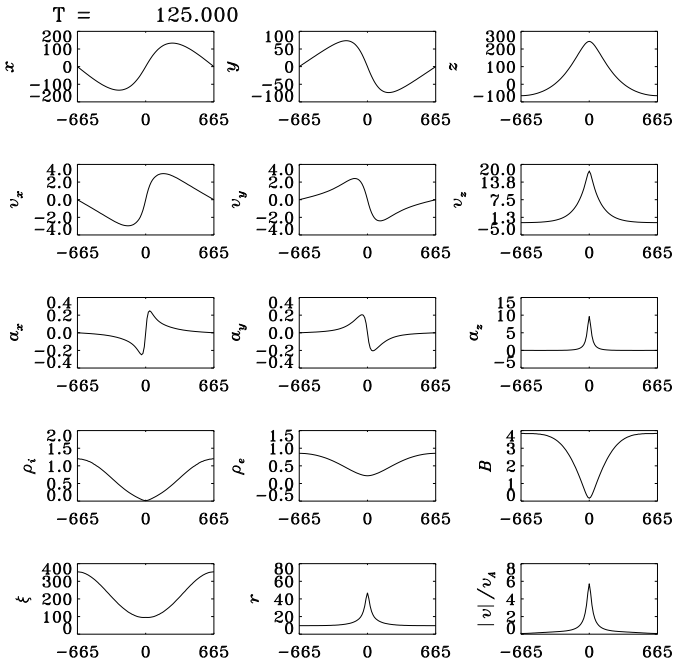

Fig. 3. The snapshot of the most relevant physical variables vs. position along the flux tube s, short before the brake down of the simulation. The basic parameters are: $\Omega = \Omega_G$, $A = 0$, $\alpha = \beta = 1$, $\lambda = 1330$ pc and $C_D = 0$ The units are: pc, Myr, 1H-atom/cm^3 and μG. The plotted quantities are: the components of displacement, velocity and acceleration, internal and external densities ρ_i, ρ_e, the internal magnetic field, mass per unit length ξ, radius of the flux tube r and the ratio of the modulus of velocity to the Alfven speed $|v|/v_A$.

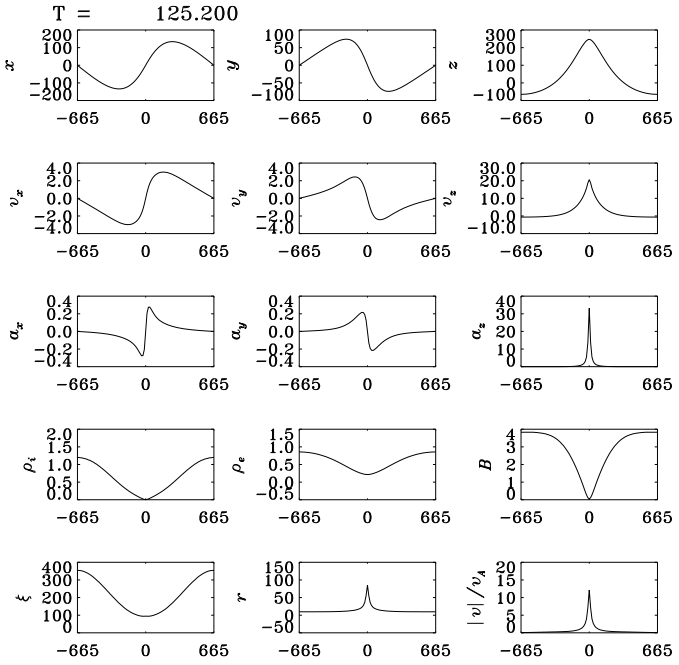

Fig. 4. The same as in previous figure 0.2 Myr later, but still before the break down.

gas density rapidly approaches zero. Since the buoyancy force is still nonvanishing and the internal mass density becomes infinitely small, the vertical acceleration has to become infinitely large. We propose to call the effect described above as a *top singularity* for brevity.

There are however weak points of the presented scenario. The magnetic flux is conserved, the magnetic field diminishes together with the internal gas density in such a way that the internal Alfven speed grows, but the vertical acceleration grows even faster, so that the vertical speed of the top starts to exceed the internal Alfven speed (see Figs. 3. and 4., bottom-right panel). As it was already mentioned (Hartquist and Morfil, 1986; Parker 1992) the bulk streaming speed of the cosmic ray gas is limited to the Alfven speed approximately, thus the assumption on the infinite streaming speed is not fulfilled in the final stages of our simulations. The limited streaming speed is difficult to incorporate quantitatively in the actual considerations, but one can expect that this effect should drastically limit the inflation rate as soon as the top speed starts to exceed the Alfven speed (the cosmic rays are not able to follow the top). Finally, the top speed should saturate at the value of the order of Alfven speed, which is large anyway.

On the other hand, the thin flux tube approximation becomes invalid in the numerical simulations as the flux tube diameter becomes comparable to the vertical scale lengths, what happens very close to the top singularity. The top singularity causes that we are not able to trace the evolution as well as the properties relevant to the dynamo theory after the moment T_{end}, even if all other parts of the flux tube in spite of its top (and its surrounding) behave regularly.

Concluding this section we can say that the top singularity is an important limitation for any numerical investigations of the Parker instability which does not take into account the limited propagation speed of cosmic rays along the magnetic field lines.

5. The dynamo coefficients

The dynamo coefficients based on our numerical simulations can be calculated with the method applied in Paper I (formulae (82) and (84)). As a first step we shall present the temporal evolution of the helicity α_d, diffusivity η_d, The magnetic Reynolds numbers R_α, R_ω and the dynamo number D for the parameter sets the same as that used in Figs. 1 and 2. This will allow us to make a first comparison of these coefficients resulting from numerical simulations to that obtained in the linear approximation in Fig. 4 of Paper I.

Fig. 5 representing the case without aerodynamic drag shows a close similarity of the behaviour of the dynamo coefficients to the results obtained in the frame of linear approximation. This similarity has been naturally expected since the evolution of the shape is very similar in both the cases of numerical simulations and the linear approxima-

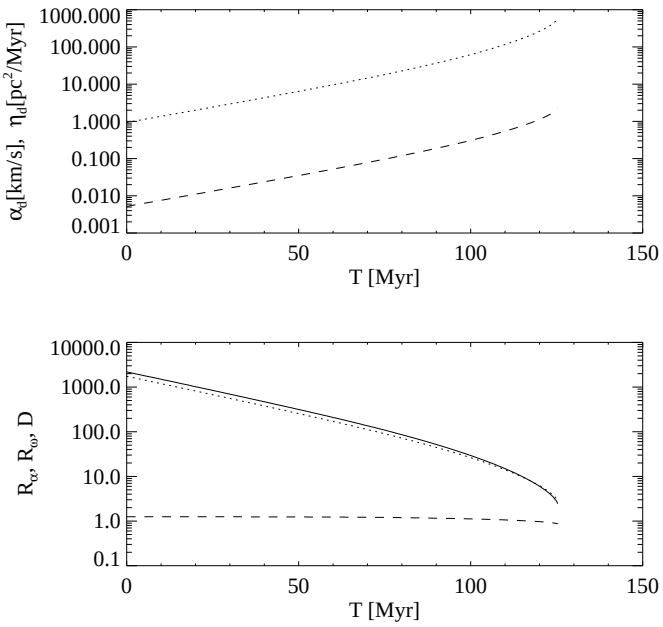

Fig. 5. The dependence of coefficients α_d (dashed line) and η_d (dotted line) on time is presented in the upper panel. The associated dynamo numbers R_α (dashed line), R_ω (dotted line) and D (full line) are shown in the lower panel. The aerodynamic drag coefficient $C_D = 0$ and the other parameters are like in Fig. 1.

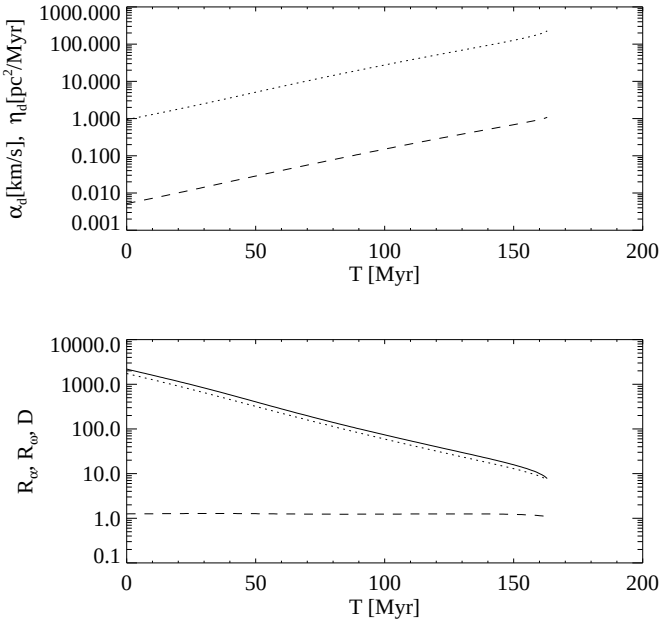

Fig. 6. The same as in Fig. 5 in except of the aerodynamic drag coefficient, which is $C_D = 1$. This case corresponds to Fig. 2. of this paper.

tion. One minor difference is apparent. Since the nonlinear growth is faster than the linear one for large amplitudes of the Parker instability, the growth of the transport coefficients α_d and η_d is faster in the nonlinear case as well.

The time dependence of the dynamo coefficients results from specific initial conditions taken into considerations: we begin with initial states of a small amplitude as described in the Section 3. We trace only the evolution of a single unstable flux tube. Since all the physical quantities involved are time dependent, the dynamo coefficients are time dependent as well. In more elaborative approach averaging over a statistical ensemble of flux tubes with a full spectrum of wavelengths and amplitudes of perturbations should be taken into account. This would allow to obtain saturated dynamo coefficients in galactic discs without density waves.

The case of the aerodynamic drag coefficient $C_D = 1$ is presented in Fig. 6. We notice that the aerodynamic drag diminishes the dynamo coefficients α_d and η_d with respect to the case $C_D = 0$, because the motion of the flux tube is slowed down.

It is now worthwhile to check if one of the main conclusions of Paper I, concerning the α-effect in the weak magnetic field limit, is still valid in the nonlinear range. We shall examine the temporal evolution of the α_d over the (α, β)-plane. The simulations have been performed for a greed 10 times 5 of parameter points, covering the range $0.0 \leq \beta \leq 1.0$ and $0.0 \leq \alpha \leq 0.5$. The choice of the wavelength maximizing the α_d coefficient has been made in the same way as in Paper I. All the simulations ended at the top singularity, while the top of the flux tube has been displaced by the distance approximately equal to the vertical scale length H. At the same time the values of the α_d were always close to 1, sometimes even larger. The results are shown in Fig. 7, where we plot α_d over the (α, β)-plane for $T = 40$ and 70 Myr. In all the simulations the initial vertical displacement amplitude is 10 pc.

We note that the results are very similar to those obtained in frame of the linear approximation. We can conclude that the strongest dynamo effect computed by means of the numerical simulations as well as in the linear approximation is reached in a timescale of a few tens of Myr for weak magnetic fields and the cosmic ray pressure comparable to the present value in the Milky Way, $p_{cr} \sim 0.5 \cdot 10^{-12}$ dyn cm^{-2}.

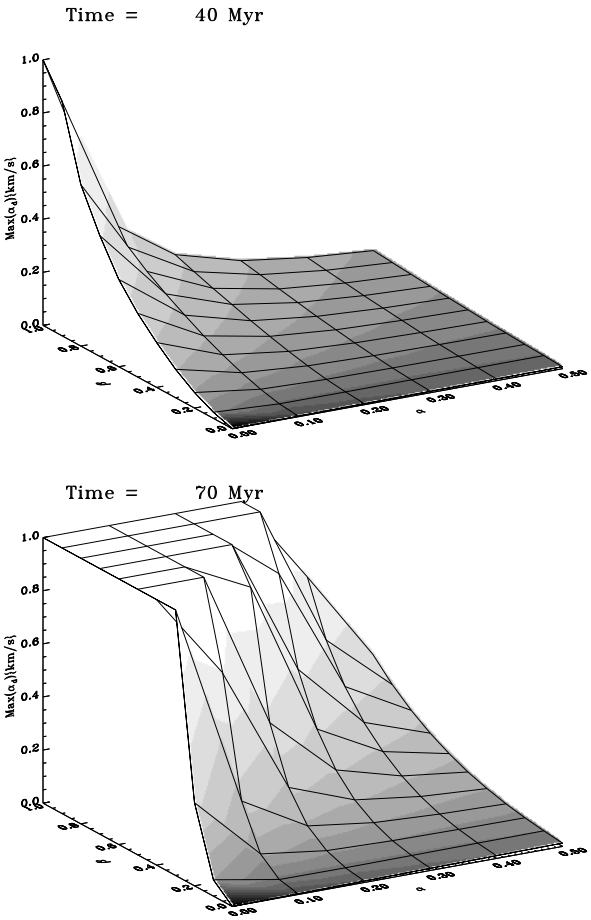

Fig. 7. The temporal evolution of the α_d coefficient over the (α, β)-plane for $T = 40$ Myr (upper panel) and $T = 70$ Myr (lower panel). Because of the top singularity we replaced the missing points with the value $\alpha_d = 1$ km/s for $T = 70$ Myr.

6. Nonlinear dynamics of magnetic flux tubes in a nonuniform external medium

We have shown in Paper I, that in the limit of weak magnetic field, the most significant contribution to the helicity α_d is due to the short wavelength modes. But these modes are more stable than the long wavelength modes which contribute to α_d only marginally (see Fig. 5 of Paper I). This leads us to the question if the generation process of magnetic field can still dominate over loses. In a more detailed description the problem looks as follows. Let us assign

$$\lambda_\alpha \equiv \lambda(\max(\alpha_d)), \tag{2}$$

for the wavelength maximizing the α_d coefficient in the linear approximation, and $\lambda_{\max}$ for a certain very large wavelength for which the growth rate is close to maximum. The respective growth rates for these wavelengths are

$$\omega_{i\alpha} \equiv \omega_i(\max(\alpha_d)), \quad \omega_{i\,\max} = \max(\omega_i). \tag{3}$$

If we deal with a mixture of linear modes of various wavelengths which start to grow with comparable initial amplitudes at $T = 0$, then the main contribution to the total α_d comes from the mode of the wavelength λ_α. In the linear approximation α_d grows with time proportionally to $\exp(2\omega_{i\alpha}t)$. On the other hand, the main contribution to the turbulent diffusivity comes from the mode of the wavelength $\lambda_{\max}$ and grows proportionally to $\exp(2\omega_{i\,\max}t)$

with $\omega_{i\,\max} > \omega_{i\alpha}$. Then it is possible that in the case of a spectrum of unstable modes, with a variety of wavelength, the losses of magnetic field associated to the long wavelength modes will become dominant over the generation process.

To check this hypothesis in the nonlinear range, for the flux tube propagating in a uniform external medium we shall perform a numerical experiment. We assume that the initial state is a composition of periodic perturbations with wavenumbers given by

$$k_n = nk_0 = \frac{2n\pi}{\lambda_0}, \tag{4}$$

where λ_0 is the maximum of wavelength determined by the size of the computational domain, and k_n are the successive wavenumbers admitted by the periodic boundary conditions. The initial perturbations are constructed in such a way that only the velocity is perturbed at $t = 0$. The initial displacements are identically equal to 0.

$$\boldsymbol{v}(s, t = 0) = \sum_{n=1}^{n_{\max}} \boldsymbol{v}_n \cos(k_n s + \varphi_n), \tag{5}$$

where $n_{\max} = 20$ is the number of periodic components and φ_n is a random phase given to each component for generality. We assume that each component has the same initial amplitude $v_n = 1$ kms^{-1} and the initial phases are generated by the random number generator. We start simulations with the above initial conditions and continue until the top singularity is reached. Then we make a plot of the shape of the fluxtube at the time directly preceding the top singularity. An example is shown in Fig. 8. We note that in spite of a compact region of strong deformation due to the Parker instability, the rest of the flux tube remains relatively straight and close to the unperturbed equilibrium state.

The temporal evolution of the dynamo coefficients for this case is presented in Fig. 9. We easily note differences with respect to the highly idealized case of the single component eigenmode initial perturbations. According to our expectations the dynamo coefficients α_d and η_d are not proportional to the same common exponential factor in the case of uniform external medium. The turbulent diffusion coefficient grows in an exponential fashion apparently, while α_d varies in a chaotic way around a value ~ 0.01 kms^{-1}, which is rather small. For this reason R_α is no longer close to a constant value, but diminishes with time. In consequence the dynamo number D diminishes much faster than R_ω. Then we note that the Parker instability would be very destructive for galactic magnetic field if the case discussed above was realistic.

The above case is not realistic however, because the interstellar medium is very non-uniform. The presence of molecular clouds is the apparent signature of this fact. We expect that the clouds perturb permanently the motion of flux tubes. If we assume, for instance, that the flux tubes

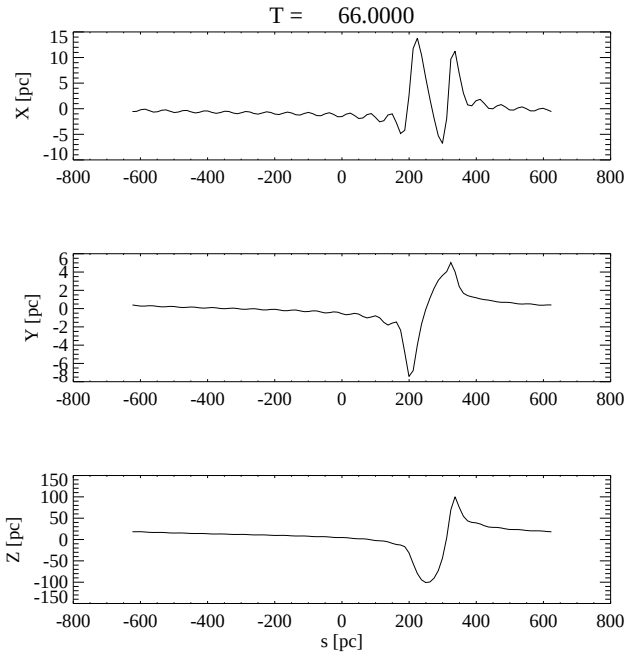

Fig. 8. The shape of the flux tube perturbed with a superposition of periodic perturbations at the moment preceding appearance of the top singularity at $T \approx 66$ Myr

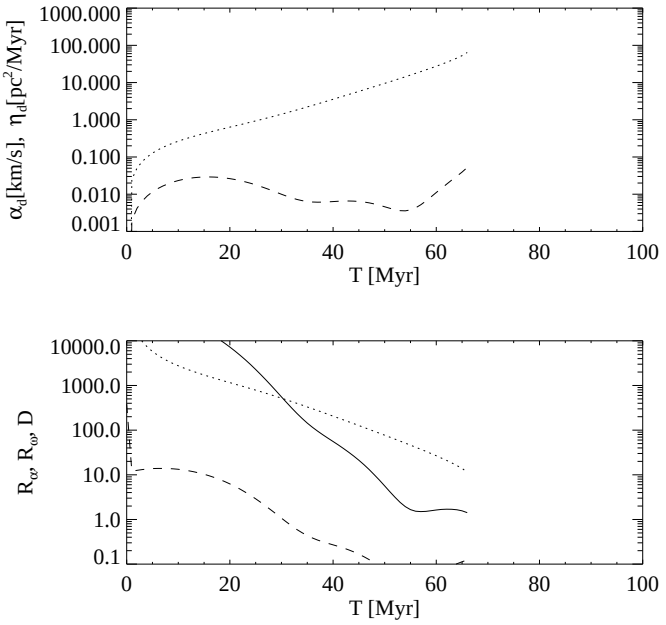

Fig. 9. The time dependence of the dynamo coefficients for the case presented in Fig. 8. Upper panel: α_d (dashed line) and η_d (dotted line). Lower panel: R_α (dashed line), R_ω (dotted line) and D (full line).

are anchored to the molecular clouds as proposed by Beck et al. (1991), (see HL'93, Paper I) then the available wavelengths of the Parker instability are related to the mean intercloud distance. The longer wavelengths of the order of galactic disc radius are suppressed due to the significant weight of molecular clouds and the escape of magnetic field by means of the very long wavelength modes is ineffective.

Alternatively, one can assume that the flux tubes are infinitely long and uniform initially, but the ambient medium is cloudy. In the forthcoming considerations we shall apply a model of the flux tube – external medium interaction, resulting from the passage of the flux tube through a medium of a nonuniform, variable density. In order to limit a number of model assumptions we do not take into account the aerodynamic drag force, which in fact could very strongly influence the flux tube motion. We assume only that the density of external medium varies in a fashion resembling a standing wave, whose maxima appear in variable places. Let us propose an analytical model of such variations taking

$$\rho_e = \rho_{e0}(z)(1+\frac{A_c}{2}(\sin(k_c s-0.5\omega_c t)-\sin(k_c s+1.5\omega_c t)) \quad (6)$$

where the amplitude of the "cloud wave" $A_c = 0.2$, and the wavelength $\lambda_c = 2\pi/k_c \sim 125$ pc, equal to the most optimal wavelength for the α-effect (see Fig. 5 of Paper I), which on the other hand is comparable to the typical intercloud distance 100 pc. The frequency of the external density modulations which we interpret as the flux tube – cloud collision frequency is

$$\omega_c = \frac{v_c}{\lambda_c} \quad (7)$$

where v_c is the typical molecular cloud speed ≈ 10 kms^{-1}. The above form of the external density modulations was incorporated in the subsequent simulation, where we applied the same initial conditions as in the simulation leading to the results presented in Figs. 8 and 9. The simulation had been continued again until the top singularity was reached at $T \sim 39$ Myr. The plot of the shape of fluxtube for this case is shown in Fig. 10. We notice that in the presence of the external density modulations, the whole length of the flux tube becomes buckled with the typical wavelength equal to the wavelength of the external density modulations, what is in contrast to the results obtained without the modulations. The temporal evolution of dynamo coefficients for this case is presented in Fig. 11.

We note the essential differences with respect to the case without the modulations of external medium:

1. The final value of the α_d coefficient is significantly larger. Without external modulations we obtained $\alpha_d \sim 0.05$ kms^{-1}, while with modulations it is ~ 0.2 kms^{-1}. The final value of the η_d coefficient is approximately the same as in the case without external modulations.

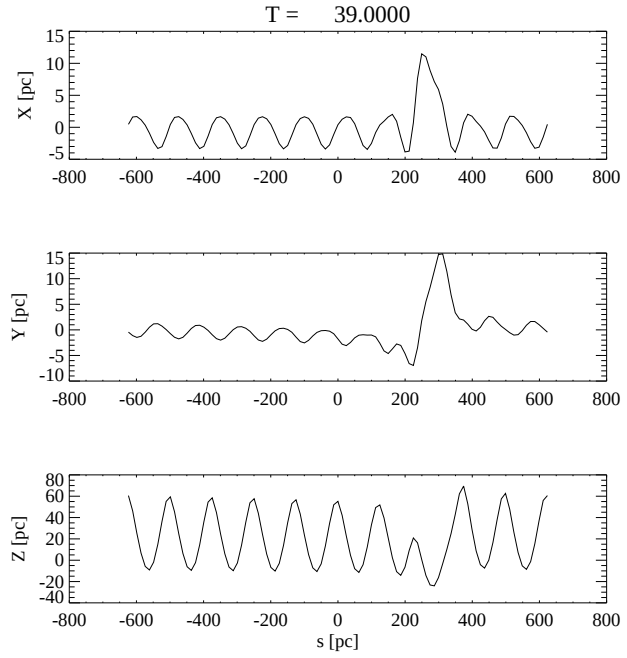

Fig. 10. The same as in Fig. 8, but with modulations of external density.

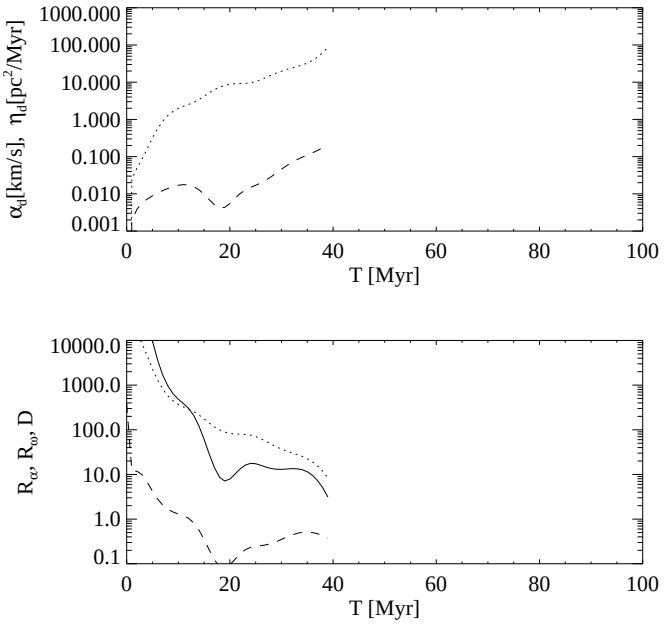

Fig. 11. The time dependence of the dynamo coefficients for the case presented in Fig. 10. Upper panel: α_d (dashed line) and η_d (dotted line). Lower panel: R_α (dashed line), R_ω (dotted line) and D (full line).

2. After an initial transient period of about 20 Myr, the transport coefficients α_d and η_d grow with a similar rate. This means that modes of the same growth rate contribute to the both α-effect and the turbulent diffusivity.
3. The final value of the R_α coefficient is ≈ 0.5 while without modulations it was ≈ 0.1. Let us recollect that R_α contains the ratio α_d/η_d, hence the generation rate of radial magnetic field is much more effective compared to losses in the presence of external modulations.

We can summarize then the role of the modulations of external medium as very favorable for the dynamo action. This is because the long wavelength modes, which are the most unstable in the linear approximation, (we consider now the weak magnetic field limit) do not dominate in the presence of the density modulations of external medium. The α-effect is strong due to the dominance of short wavelength modes.

7. The effect of rotational shear

In this section we present the results of numerical simulations taking into account the differential force resulting from the rotational shear ($F_{diff} = -4A\Omega\rho$). As it has been described in Paper I the magnitude of shear is parameterized by the Oort constant A, which is equal to 0, -1/2 and -3/4 for rigid, flat and Keplerian rotation curves respectively. The parameters of the simulations are: $\alpha = \beta = 1$, $\Omega = \Omega_G$. We fix the wavenumber $k_0 = k_{crit} = 0.0044$ pc^{-1} ($\lambda_{crit} = 1430$ pc) for ($A = -1/2$). Whereas the wavenumber of perturbations is fixed, we shall vary the shearing parameter A around $A_0 = -1/2$ corresponding to the flat rotation curve. In Paper I we have shown that the density waves introduce an additional differential force. The differential force corresponding to the linearity limit of the interstellar gas perturbations is equivalent to oscillations of A with the 'top-bottom' amplitude equal to about 50 % of $|A_0| = 1/2$. This linearity limit is related to a very small (1%) spiral density wave perturbation of the axisymmetric gravitational potential.

Let us take for simplicity two fixed values $A_1 = -3/8$ and $A_2 = -5/8$ of the Oort constant A. The two values are placed symmetrically around A_0 and their difference equals 50% of A_0. For A_1 the perturbation with k_0 is placed in the Parker range, while for A_2 in the shearing range. We shall perform two complementary runs of numerical simulations for these two values of the Oort constant. Our aim is to figure out the qualitative differences between these two cases, considering the basic physical variables already displayed in Figs. 3 and 4, and the dynamo coefficients, as well.

Let us focus on the shape of the flux tube and the related variables first. We shall analyze late stages of the evolution of the Parker-shearing instability, which precede the appearance of the top singularity by less than 5 Myr. The results are presented in Figs. 12 and 13.

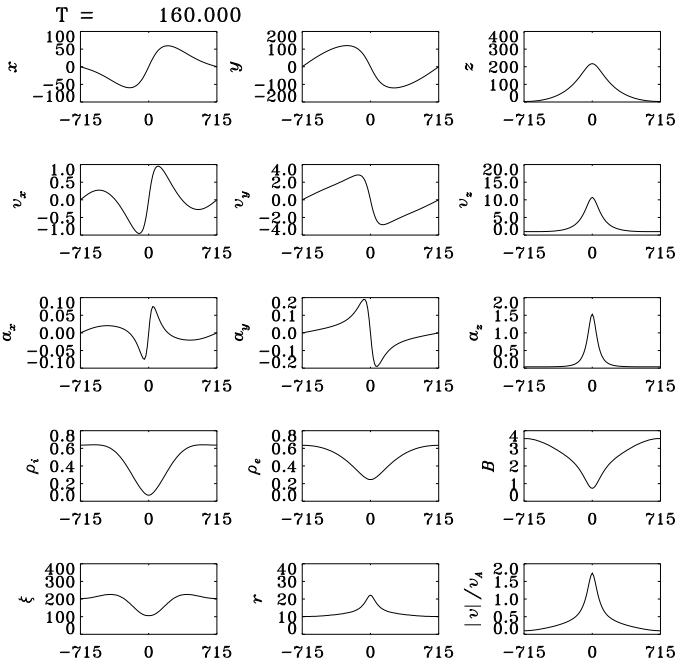

Fig. 12. The snapshot of the most relevant physical variables vs. position along the flux tube for the Parker range ($A = A_1 = -3/8$, $\lambda = \lambda_{crit} = 1430$ pc for $A_0 = 1/2$). The other parameters and units are the same as in Fig. 3

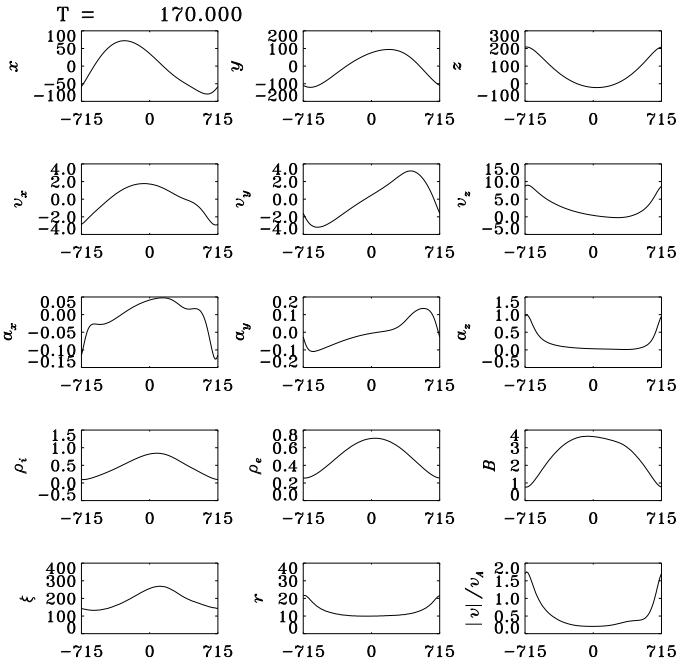

Fig. 13. The snapshot of the most relevant physical variables vs. position along the flux tube for the shearing range ($A = A_2 = -5/8$, $\lambda = \lambda_{crit} = 1430$ pc for $A_0 = 1/2$). The other parameters and units are the same as in Fig. 3

In Fig. 12 ($A = A_1$, k_0 is in the Parker range) we note a regular, symmetric shape of the flux tube with apparent signatures of some nonlinear departures from the sinusoidal shape. The central part of the azimuthal displacement X-curve is steepened, the top of Z-curve is vertically peaked and the bottom is shifted above the initial vertical position of the flux tube. In the linear regime the bottom displacement is negative and its absolute value is the same as the vertical displacement of the top. In contrast to the case without shear, the azimuthal velocity curve V_x becomes double periodic, what means that gas does not flow toward the lowest point of the flux tube at its lower parts, but instead it flows toward two points placed in between the top and the bottom. This is confirmed by the shape of the curve representing the mass per unit length of the flux tube ξ. We note two points of the gas concentration in between the positions of the top and bottom. The values of ρ_i approaching 0 mean that the presented stage of the flux tube evolution is close to the top singularity and the assumptions of the thin flux tube approximation start to be violated near the top of the flux tube. The $|v|/v_A$ exceeding 1 means that the transport of cosmic rays along the magnetic field lines starts to be inefficient to inflate freely the topmost parts of the flux tube.

In Fig. 13 ($A = A_2$, k_0 is in the shearing range) we note that the shape of the flux tube becomes irregular. We have demonstrated in Paper I that the solutions are the propagating waves in this range, so that the azimuthal position of the top is shifted with respect to its initial position at $s = 0$. The phase shift between the y- and z-displacements is less favorable for the magnitude of the α_d coefficient than in the Parker range. In the linear range the formula for α_d contains the quantity $\mathrm{Im}(\mathrm{Y_1/Z_1})$ (the imaginary part of radial to vertical displacement amplitude ratio), which is the largest for the phase difference about $\pm\pi/2$ between the vertical and horizontal displacements. Since this case represents the shearing range, α_d is significantly reduced with respect to the Parker range as it is shown in Fig. 8 of Paper I. From the graph presenting the distribution of mass per unit length ξ we learn that gas concentrates around a single point, which is maximally displaced in the positive y (radial) direction. Simultaneously this is the lowest point on the flux tube. The point maximally displaced in the negative y direction has the lowest linear mass density and is the highest point of the flux tube. Similarly to the previously discussed case of $A = A_1$, the presented stage of the flux tube evolution is at the limit of applicability of the used approximations.

Comparing the above two cases we can say that the final mass distribution along the flux tube is a result of compromise between two different redistributing forces: the gravitational force, which tends to place gas in the lowest point of the flux tube and the differential force, which tends to place gas in the points which are extremely displaced in the radial direction. In the Parker range (the differential force is relatively weak), the two mass concentrations appear without a modification of the phase relations between the displacements in three spatial directions. For the stronger differential force in the shearing range the phase relations are modified and the two categories of concentration points merge (i.e. the bottom becomes maximally displaced in the radial direction). This effect diminishes the dynamo α-effect forcing the disadvantageous phase relation between the radial and azimuthal displacements. It appears, however, that a residual α-effect remains in the shearing range, but it is much weaker than the α-effect in the Parker range.

The temporal evolution of the dynamo coefficients for both the cases of Parker-shearing instability is presented in the subsequent Figs. 14 and 15, which are complementary to Figs. 12 and 13 respectively. We note that α_d is apparently larger in the Parker range (Fig. 14) than in the shearing range (Fig. 15), what confirms the previous results obtained in the linear regime. It is worth noting, however, that the dominance of the α-effect in the Parker range diminishes slightly during the nonlinear evolution of the Parker-shearing instability. The diffusivity η_d behaves very similarly in both the cases because the growth rates are very similar. This implies the similarity of the magnetic Reynolds number R_ω. The magnetic Reynolds number R_α and in consequence the dynamo number D are larger in the Parker range than in the shearing range following the same behaviour of α_d.

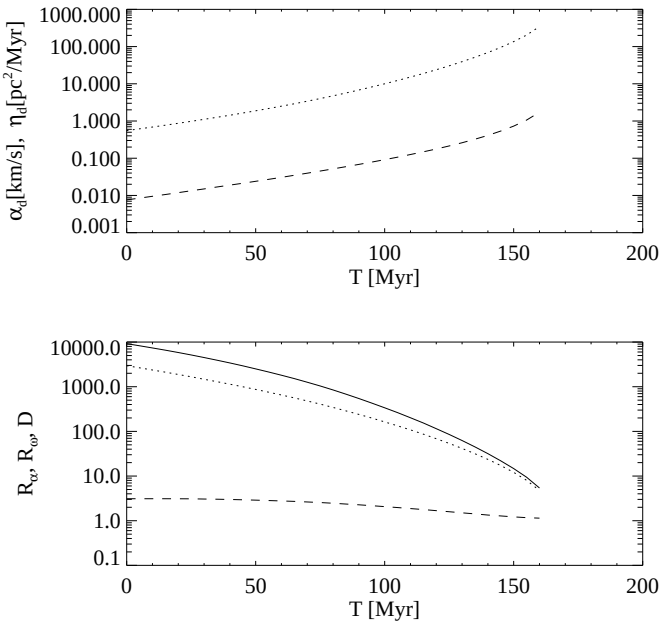

Fig. 14. The time dependence of the dynamo coefficients for the Parker range ($A = A_1$). Upper panel: α_d (dashed line) and η_d (dotted line). Lower panel: R_α (dashed line), R_ω (dotted line) and D (full line).

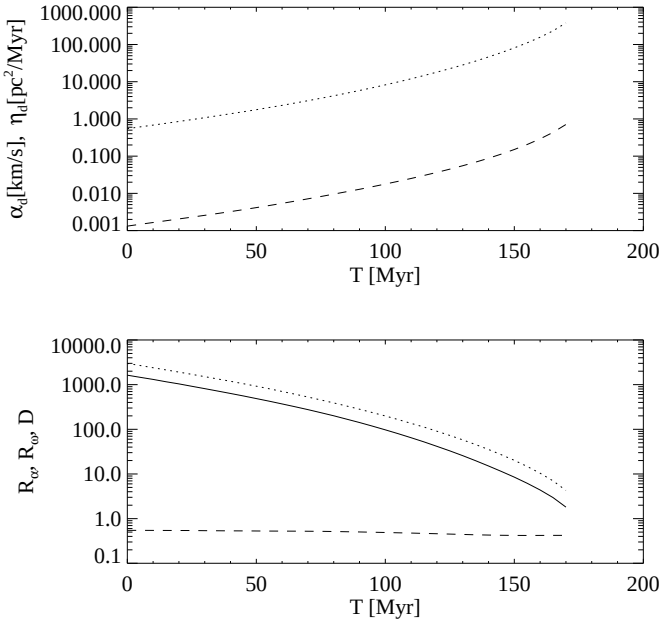

Fig. 15. The time dependence of the dynamo coefficients for the shearing range ($A = A_2$). Upper panel: α_d (dashed line) and η_d (dotted line). Lower panel: R_α (dashed line), R_ω (dotted line) and D (full line).

We can conclude that the nonlinear numerical simulations well confirm our previous linear results of Paper I, with the exception that the difference of α_d between the Parker and shearing ranges becomes less pronounced in the nonlinear range.

8. Discussion and Conclusions

In this paper we present the results of numerical simulations solving the nonlinear system of partial differential equations, derived in Paper I for the dynamics of magnetic flux tubes in galactic discs. The obtained numerical solutions appeared to be very consistent with the linear analytical solutions derived in Paper I for amplitudes of vertical displacements of the flux tubes smaller than the vertical scale length H. This consistency between the numerical and the analytical results allows us to confirm the previous conclusion: the weak magnetic field enables the fast growth of Parker instability and the strong dynamo action due to the weakness of magnetic tension if only the cosmic ray pressure is high enough.

An essential advantage of the performed simulations follows from the fact that we have been able to trace the nonlinear evolution of the Parker unstable flux tubes. We have shown that due to the contribution of cosmic rays the top of the flux tube inflates rapidly at finite vertical displacements of the order of vertical scaleheight H. This gives rise to an enormous growth of the vertical buoyancy acceleration. This process is able to form the vertical structure of magnetic field lines extending to the galactic halo, as it is observed in some cases of edge-on galaxies like NGC 4631 (Hummel et al. 1991; Golla and Hummel 1994) and M82 without any additional driving force. We note however that the inflation rate should be reduced if only the streaming speed of cosmic rays along the magnetic field lines is limited, so that the velocities of vertical rise should saturate at the level comparable to the Alfven speed, typically several tens to hundreds of km/s. The last estimation depends on the particular values of the magnetic field strengths and gas densities, so that large variations of the Alfven speed are possible depending on galaxy.

Reuter et al. (1992, 1994) point out that the halo of M82 is characterized by a filamentary structure with prominent gaps localized between these filaments. These features exhibit a preferential orientation normal to the plane of M82 and extend out to z-distances of $\simeq$ 1 kpc. The linear polarization up to 35 % was found there with the polarization degree increasing with z-distance. Moreover, the vertical dependence of the spectral index of synchrotron radiation was interpreted as an evidence, that the relativistic plasma is streaming into the halo along vertical magnetic field lines with velocities in excess of 1000 kms^{-1}. The M82 galaxy is known for its intense star formation activity at the center, what implies the intense production of cosmic rays, which are so important for our model. We can say that even if the Parker instability is not easily separable from the other effects like galactic winds and galactic fountains, the presented observational picture of the mentioned galaxies is consistent with our theoretical model. We would like to point out that we can explain the vertical magnetic field structure of M82, the streaming of cosmic ray gas with very large vertical velocity as well as the generation of magnetic field within a single model of galactic dynamo driven by the Parker instability.

We have made a point in this paper that if the cosmic ray pressure significantly exceeds the magnetic pressure, the Parker instability is able to produce an effective dynamo action. This is possible if 1) the flux tubes are anchored in molecular clouds with mean separation comparable to the most optimal wavelength for the α-effect (see Paper I), or 2) the flux tubes propagate in the nonuniform external medium as it has been discussed in this paper. Taking into account an exemplary model of weak modulations of the external medium density we have shown that the dominating wavelengths of the buckling of flux tubes is the same as the wavelength of modulations of the external medium. We attribute these modulations to the presence of molecular clouds with typical separation of 100 pc. With these modulations the dynamo α-effect is essentially stronger than without the modulations and strong in comparison to the vertical diffusion of magnetic field. Without these modulations the diffusion rate tends to dominate over the generation rate.

Performing numerical simulations of the nonlinear evolution of flux tubes we have examined the role of the galactic differential forces resulting from the axisymmetric differential rotation for two distinct values of the Oort constant A. These simulations allowed us to figure out the qualitative differences between the Parker and the shearing ranges introduced in Paper I. We have found that for given perturbation with wavenumber k_0, in the Parker range (weak shear) of the Parker-shearing instability, the qualitative properties are similar to the case without shear. There is, however, an effect resulting from the presence of the radial differential force – the gas starts to gather not at the lowest point of the flux tube, but at two points extremely displaced in the radial direction. In contrast, we note a drastic change of the general behaviour of the instability in the shearing range. The perturbations become propagating waves. The gas starts to gather around one point, which is the lowest one and simultaneously the most displaced in the radial direction. This qualitative change implies the modification of the phase difference between the radial and the vertical displacements. This effect in turn is responsible for the drop of the dynamo α_d coefficient. In the nonlinear regime the α-effect is still much more effective in the Parker range than in the shearing range, but the jump of its magnitude is smaller than that obtained in the linear regime. Following Paper I we associate the Parker range with the enhanced α-effect with the spiral arms. Similarly we associate the shearing range with the diminished α-effect with the interarm regions. We note that a more elaborated approach should take into account the higher cosmic ray production rate in spiral arms, which should additionally magnify the contrast of the α-effect between arms and the interarm regions.

Summarizing, we can say that all the numerical simulations well confirm our former results of Paper I, and additionally highlight the new nonlinear aspects. In Paper I we proposed a new model of galactic dynamo which is a cyclic process involving the action of the Parker-shearing instability, galactic differential rotation, density waves and magnetic reconnection. In this model the α-effect of the $\alpha\omega$ dynamo is essentially dependent on the phase of the galactic density wave and is localized in spiral arms. The complementary shear (the ω-effect) is enhanced in the interarm regions. The dissipation process necessary for the dissipation of the small scale nonuniform magnetic field components is accomplished by the magnetic reconnection. Our dynamo model is a kind of a fast dynamo proposed by Parker (1992), which is free of problems pointed out by Kulsrud and Anderson (1992).

Our approach, based on nonlinear dynamics of flux tubes, allowed us to compute the dynamo transport coefficients with the back reaction of the large scale magnetic field taken into account. We found that the presence of cosmic rays and the rotational differential force allow to overcome magnetic tension, so that the dynamo transport coefficients do not saturate under the influence of magnetic field of the strength below the observed equipartition value. Thus, our model avoids the basic problems of mean field dynamos as described by Vainshtein and Cattaneo (1992).

Acknowledgements. I wish to thank prof. Harald Lesch and prof. Marek Urbanik for their useful comments. This work was supported by the grant from Polish Committee for Scientific Research (KBN), grant no. PB 0479/P3/94/07.

References

Asseo, E., et al. 1978, ApJ 225, L21
Asseo, E., et al. 1980, ApJ 237, 752
Beck, R., Berkhuijsen, E.M., Bajaja E., 1991, in *Dynamics of Galaxies and Molecular Cloud Distribution*, IAU Symp. 146, F. Combes, F., Casoli (eds.)
Beck, R., Hoernes, P., 1996, Nature, 379, 47
Hanasz, M., Lesch, H., 1993, A&A 278, 561
Hanasz, M., Lesch, H., 1996, A&A 321, 1007, Paper I, astro-ph/9610167
Hartquist, T.W., Morfill, G.E., 1986, ApJ 311, 518
Hummel, E., Beck, R., Dahlem, M., 1991, A&A 248, 23
Kahn, F.D., Brett, L., 1993, MNRAS 263, 37
Lechieze-Rey, M., et al., 1980, ApJ 238, 175
Kulsrud, R.M., Anderson, S.W., 1992, ApJ 396, 606
Madsen, N.K., Sincovec, R.F., 1992, ACM-TOMS 18, 343
Moreno-Insertis, F., 1986, A&A 166, 291
Mouschovias, T.Ch., 1974, ApJ 192, 37
Mouschovias, T.Ch., 1975, A&A 40, 191
Parker, E.N., 1979, *Cosmical magnetic fields*, Oxford
Parker, E.N., 1992, ApJ , 401 137
Reuter, H.-P., Klein, U., Lesch, H. et al., 1992 A&A 256, 10
Reuter, H.-P., Klein, U., Lesch, H. et al., 1994 A&A 282, 724
Shu, F.H., 1974, A&A 33, 55
Spencer, S.J., Cram, L.G., 1992, ApJ 400, 484
Spruit, H.C., 1981, A&A 98, 155
Spruit, H.C., Van Ballegooijen, A.A., 1982, A&A 106, 58
Vainshtein, S.I., Cattaneo, F., 1992, ApJ 393, 165

This article was processed by the author using Springer-Verlag LaTeX A&A style file *L-AA* version 3.